Journal of Computational Physics 228 (2009) 8203–8213

Contents lists available at ScienceDirect

Journal of Computational Physics

journal homepage: www.elsevier.com/locate/jcp

On discretization errors and subgrid scale model implementations in large eddy simulations

A. Viré *, B. Knaepen

Physique Statistique et des Plasmas, Faculté des Sciences, Université Libre de Bruxelles, Campus Plaine – CP231, Bd. du Triomphe, B-1050 Brussels, Belgium

ARTICLE INFO

Article history:
Received 8 July 2008
Received in revised form 13 November 2008
Accepted 12 December 2008
Available online 30 December 2008

Keywords:
Large eddy simulation
Finite volume method
Smagorinsky model
Homogeneous isotropic turbulence

ABSTRACT

We analyze the impact of discretization errors on the performance of the Smagorinsky model in large eddy simulations (LES). To avoid difficulties related to solid boundaries, we focus on decaying homogeneous turbulence. It is shown that two numerical implementations of the model in the same finite volume code lead to significantly different results in terms of kinetic energy decay, time evolutions of the viscous dissipation and kinetic energy spectra. In comparison with spectral LES results, excellent predictions are however obtained with a novel formulation of the model derived from the discrete Navier–Stokes equations. We also highlight the effect of discretization errors on the measurement of physical quantities that involve scales close to the grid resolution.

1. Introduction

The aim of large eddy simulations is to reproduce with accuracy the large scale properties of a turbulent flow at a much lower computational cost than required by direct numerical simulations (DNS). By definition, LES are thus performed on coarse meshes that do not capture the small scales which are present in the actual flow. These *subgrid scales* are nevertheless important and strongly influence the dynamics of the large *resolved scales*. The main challenge of LES is then to appropriately model the influence of the subgrid scales on the resolved scales through a *subgrid scale (SGS) model*. On these grounds, SGS modeling is largely a physics problem that needs to take into account the nature of turbulence and in particular the cascade of energy from large to small scales through the inertial range. This viewpoint is supported by Kolmogorov's universality theory which implies that the statistical properties of turbulence are universal in the inertial range at large Reynolds numbers.

The numerical method that is most faithful to the LES paradigm is of course the spectral method. Focusing on homogeneous turbulence, the resolved velocity field can indeed be developed on the basis of Fourier modes limited to wave vectors up to a given cut-off. Hence, the neglected modes unambiguously define the subgrid scales. The LES equations are also perfectly well defined since all spatial derivatives can be computed exactly by multiplication of the Fourier modes with the appropriate powers of the wave vector. In the absence of explicit filtering (for example with a Gaussian or top-hat filter), the physical problem of subgrid scale modeling is then completely free of *discretization* errors.

In practice, the flow configurations are usually much more complex. For problems in wall-bounded or complex geometries, one usually resorts to other spatial discretizations of the Navier–Stokes equations. Here, the attention is restricted to finite volume methods, although the present arguments can be applied to other techniques like finite elements or finite difference schemes. Ultimately, the flow is simulated using a finite number of discrete variables located at a given set of grid

* Corresponding author.
E-mail address: avire@ulb.ac.be (A. Viré).

0021-9991/$ - see front matter © 2008 Elsevier Inc. All rights reserved.
doi:10.1016/j.jcp.2008.12.024

points. For finite volume schemes, these variables represent the velocity and pressure fields averaged over control volumes of typical size Δ. In LES, Δ is obviously quite large in order to limit the computer requirements. If we exclude explicit filtering, the filtering operation which requires subgrid scale modeling can then be identified with the volume averaging on the coarse mesh (this averaging is responsible for the destruction of small scale information). However, because the mesh is coarse, the discrete operators needed for differentiations and interpolations introduce further errors that might be very significant. For differentiation operators, the severity of this problem increases with the order of the derivative taken. In that case, the physical relevance of the numerical results becomes questionable.

Several previous studies highlighted the interplay between discretization errors and subgrid modeling. The first systematic analyses of discretization errors in large eddy simulations are due to Vreman et al. [1] and Ghosal [2]. In the latter, the author analyzed finite difference operators in homogeneous isotropic turbulence and showed that discretization errors could be of equal importance as the subgrid scale model's contribution. To overcome this problem, the author recommends the use of higher-order discretization schemes or the explicit filtering of the LES field to damp scales close to the grid size. This study was extended to the case of stratified sheared turbulence where LES discretization errors were analyzed using data obtained from high resolution DNS [3].

The use of high-order methods is very demanding in terms of implementation and computational costs. For this reason, many studies have focused on the application of explicit filters in low-order methods with the aim of minimizing the influence of numerical errors. As explained in [4], the distinction between discretization and explicit filtering is then essential. Discretization is responsible for a loss of information and ultimately leads to a closure problem (this is made clear by considering the discretizing operators as "filters" [5]). This contrasts with explicit filters that can be formally taken into account by using a power series in the filter width (at least for a certain class of filters). The benefit provided by explicit filtering still remains unclear [6]. In particular, Lund [7] showed that a grid refinement with traditional models (i.e. without explicit filtering) may lead to better results than the use of an explicit filter in two directions. Furthermore, explicit filtering introduce difficulties related to the commutation error between the filter and differentiation operators [8]. Nevertheless, a revived interest in explicit filters has appeared in relation to "variational multiscale models" in which scales close to the grid size are separated from the rest of the resolved scales to determine the subgrid scale model [9,10].

Other studies have focused on the minimization of the total error (i.e. sum of modeling and discretization errors) and its dependence on numerical and physical settings [11–14]. As also observed by [15], the reduction of one component (or both) of the error may not necessary lead to a decrease of the total error. Hence, this may yield counter-intuitive effects and poses the question of quality and reliability of LES predictions [14].

The purpose of this paper is twofold. We first compare two implementations of the Smagorinsky subgrid scale model in a finite volume code. These implementations differ only in terms of the model discretization and we use a spectral LES (without explicit filtering) as the benchmark case. It is found that the performance of the model largely depends on the discretization adopted and we advocate the use of a discretization which is derived from the discrete implementation of the Navier–Stokes equations. Some filtered DNS results are also presented but only for illustrative purposes. They are deliberately not used as the main benchmark since we do not focus on the intrinsic performance of the Smagorinsky model but only on how to implement the analytical form as faithfully as possible in a numerical code. In that respect, comparison with a spectral LES is more appropriate whereas comparison with a filtered DNS is more suitable to test the physical content of a model.

The second objective of this work is to bring the attention on the ambiguity, resulting from discretization errors, of physical results extracted from LES on coarse meshes. We stress that the conclusions of this study are applicable to finite element or finite difference schemes without any significant changes. Also, to avoid having to deal with the resolution of boundary layers, we limit our attention to homogeneous turbulence. This further allows a detailed comparison with an accurate spectral solver.

The manuscript is organized as follows. The second-order finite volume LES solver is presented in Section 2. Using kinetic energy budgets, the performance of two implementations of the Smagorinsky subgrid scale model is compared in Section 3. In Section 4, we comment on the importance of discretization errors in the measurement of physical quantities involving length-scales close to the grid size. Finally, our conclusions are presented in Section 5.

2. Numerical method and subgrid modeling

2.1. Numerical discretization

The computations are performed using the CDP code developed at the Center For Turbulence Research (Stanford/ NASA Ames). This code uses a collocated discretization of the incompressible Navier–Stokes equations in a node-based formulation. A typical grid element is illustrated in Fig. 1. The label C corresponds to the location of the centroid of the element in the original volume-based grid. In the dual mesh, the node-based control volumes are centered around each of the vertices (nodes) of this original mesh. In the figure, P represents such a node of the dual mesh. The velocity and pressure fields are stored at these nodes and the (independent) face normal velocity U_f are stored at the centroid of the dual volume's faces.

The details of the code are described extensively in [16–18], and therefore, only the information relevant to the present study is reported here. The LES equations derived from the incompressible Navier–Stokes equations are solved using the following fractional step method:

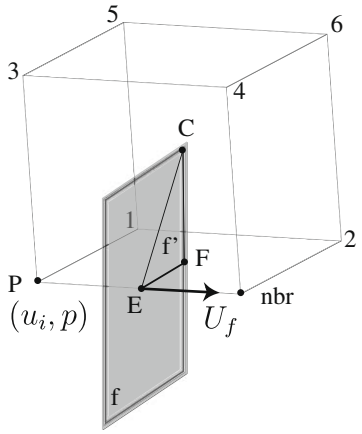

Fig. 1. Illustration of the collocated mesh. The shaded area represents a face belonging to the mesh dual to that defined by the original grid centroids.

$$\frac{\hat{\bar{u}}_{i,P} - \bar{u}^n_{i,P}}{\Delta t} V_P + \sum_f \overline{U}^{n+1/2}_f \bar{u}^{n+1/2}_{i,f} A_f = -(\partial_i \bar{p})^{n-1/2}_P V_P + \sum_f \nu(\partial_i \bar{u}^n_j + \partial_j \bar{u}^{n+1/2}_i)_f \beta_{j,f} A_f + \text{SGS term} \tag{1}$$

$$\frac{\bar{u}^{\star}_{i,P} - \hat{\bar{u}}_{i,P}}{\Delta t} = (\partial_i \bar{p})^{n-1/2}_P, \tag{2}$$

$$\frac{\bar{u}^{n+1}_{i,P} - \bar{u}^{\star}_{i,P}}{\Delta t} = -(\partial_i \bar{p})^{n+1/2}_P, \tag{3}$$

where the last term of the right-hand-side of (1) represents the subgrid scale contribution (see below for more details). In the above equations, V_P is the volume of the control volume surrounding point P and the sums are extended to all faces f delimiting this control volume. The face areas are denoted A_f and their unit normal vectors are written $\beta_{i,f}$. Variables have the subscripts P or f depending on whether they are evaluated at the center of the control volume or the face. We further have the time integration expressions: Adams–Bashforth,

$$\overline{U}^{n+1/2}_f = \frac{3}{2}\overline{U}^n_f - \frac{1}{2}\overline{U}^{n-1}_f, \tag{4}$$

and Crank–Nicholson,

$$\bar{u}^{n+1/2}_{i,f} = \frac{1}{2}(\hat{\bar{u}}_{i,f} + \bar{u}^n_{i,f}). \tag{5}$$

In order to fully close Eq. (1) (barring the definition of the subgrid scale contribution), the interpolation schemes from nodal to face quantities have to be specified. Once a quantity ϕ is known at two neighboring nodes, it is interpolated to the mutual face (see Fig. 1) as

$$(\phi)_f = \frac{\phi_P + \phi_{nbr}}{2}. \tag{6}$$

In order to evaluate the gradients, two schemes will be compared. Both make use of the discrete Gauss theorem but they give different interpolations.

- The first scheme leads to a central difference discretization (CDS) of the node derivative:

$$(\partial_j \phi)_P V_P = \sum_f \frac{\phi_P + \phi_{nbr}}{2} \beta_{j,f} A_f. \tag{7}$$

- The second scheme expresses the derivative as a summation-by-part (SBP) operator [18]:

$$(\partial_j \phi)_P V_P = \sum_f \sum_{f'} \phi_{f'} \beta_{j,f'} A_{f'}. \tag{8}$$

In the SBP scheme, each control volume's face is decomposed into subfaces f'. In Fig. 1, the shaded area represents one face of the control volume centered around node P, and is divided into eight subfaces, one of which is for example f'. For a mesh consisting of quadrilaterals, each subface is a triangle. The variable ϕ_f at the face results in an average of its values $\phi_{f'}$ at the subface's centers. Moreover, for the cartesian mesh illustrated by Fig. 1, $\phi_{f'} = (\phi_E + \phi_F + \phi_C)/3$, $\phi_E = (\phi_P + \phi_{nbr})/2$, $\phi_F = (\phi_P + \phi_{nbr} + \phi_1 + \phi_2)/4$ and $\phi_C = (\phi_P + \phi_{nbr} + \phi_1 + \phi_2 + \phi_3 + \phi_4 + \phi_5 + \phi_6)/8$.

The only face-centered gradient that is not computed through (7) or (8) is that related to the second part of the viscous term. It represents the largest contribution to the viscous stress and can be treated more accurately using the following semi-implicit decomposition:

$$(\partial_j \bar{u}_i^{n+1/2})_f \beta_{j,f} = \frac{\bar{u}_{i,nbr}^{n+1/2} - \bar{u}_{i,P}^{n+1/2}}{\|x_{j,nbr} - x_{j,P}\|}. \tag{9}$$

Eq. (3) is used to compute the pressure at step $n+1/2$ through the Poisson system defined by the incompressibility condition,

$$(1/\Delta t) \sum_f \bar{u}_{i,f}^{\star} \beta_{i,f} A_f = \sum_f (\partial_\beta \bar{p})_f^{n+1/2} A_f. \tag{10}$$

Once the nodal pressures are determined through (10), the nodal and face normal velocities are updated using:

$$\bar{u}_{i,P}^{n+1} = \bar{u}_{i,P}^{\star} - \Delta t (\partial_i \bar{p})_P^{n+1/2}, \tag{11}$$

$$\overline{U}_f^{n+1} = \overline{U}_f^{\star} - \Delta t (\partial_\beta \bar{p})_f^{n+1/2}. \tag{12}$$

In (10), the velocity is interpolated at the neighboring nodes following (6) and the pressure gradient at the face is computed using a similar expression as (9). Thus, the velocity and pressure fields are evaluated using the same nodes (i.e. the neighboring nodes P and nbr of a given face f) and there is no odd-even decoupling in the algorithm [17]. This procedure however introduces an implicit dissipation, which is proportional to the time step and the square of the mesh spacing. In the present study, we have reduced the time step so that the artificial dissipation is two orders of magnitude smaller than the physical dissipations (see [17] for details).

2.2. Subgrid scale model

The last ingredient that needs to be specified is the subgrid scale contribution appearing in (1). We focus here on the widely used Smagorinsky model based on the eddy viscosity concept [19] so that the SGS term is written as:

$$\sum_f (\nu_e^n)_f (\partial_i \bar{u}_j^n + \partial_j \bar{u}_i^{n+1/2})_f \beta_{j,f} A_f, \tag{13}$$

with,

$$\nu_e = -2C\overline{\Delta}^2 \mid \overline{S} \mid, \quad \mid \overline{S} \mid = \sqrt{2\overline{S}_{ij}\overline{S}_{ij}}, \quad \overline{S}_{ij} = \frac{1}{2}(\partial_i \bar{u}_j + \partial_j \bar{u}_i). \tag{14}$$

Since we focus on isotropic turbulence, we choose $C = 0.0225$ [20] and $\overline{\Delta} = L_x/N_x$ with L_x and N_x being, respectively, the computational box size and the number of cells in one of the directions (the mesh is isotropic).

Simulations are performed using two discretization schemes for $(\nu_e^n)_f$. In both cases, the face-centered turbulent viscosity is obtained from nodal values through (6).

The first implementation of the turbulent viscosity is

$$(\nu_{e,1}^n)_P = -2C\overline{\Delta}^2 \sqrt{2(\overline{S}_{ij}^n)_P (\overline{S}_{ij}^n)_P}. \tag{15}$$

For $(\nu_{e,1}^n)_P$, each strain is computed explicitly using the CDS or SBP interpolations (7) and (8). In the following, the subgrid scale model using this traditional "volume centered" eddy viscosity is referred to as SM1.

To introduce the second implementation of the turbulent viscosity, we make use of the identity:

$$\overline{S}_{ij}\overline{S}_{ij} = -\bar{u}_i \partial_j \overline{S}_{ij} + \partial_j (\bar{u}_i \overline{S}_{ij}), \tag{16}$$

which leads to the following nodal discretization $\mathcal{D}[\overline{S}_{ij}\overline{S}_{ij}]_P$ for the norm of the strain:

$$\mathcal{D}[\overline{S}_{ij}\overline{S}_{ij}]_P = -\bar{u}_{i,P}^n \sum_f \frac{1}{2V_P} (\partial_i \bar{u}_j^n + \partial_j \bar{u}_i^n)_f \beta_{j,f} A_f + \sum_f \frac{1}{2V_P} (\bar{u}_i^n)_f (\partial_i \bar{u}_j^n + \partial_j \bar{u}_i^n)_f \beta_{j,f} A_f. \tag{17}$$

The face-centered gradients $(\partial_j \bar{u}_i^n)_f \beta_{j,f}$ are again calculated using (9) (in explicit form) while the remaining gradients are computed using the CDS or SBP interpolations (7) and (8).

Based on (17), we define an alternative subgrid scale viscosity,

$$(\nu_{e,2}^n)_P = -2C\overline{\Delta}^2 \sqrt{2\mathcal{D}[\overline{S}_{ij}\overline{S}_{ij}]_P}. \tag{18}$$

Hereafter, the subgrid scale model based on this turbulent viscosity is referred to as SM2.

The main advantage of $\mathcal{D}[\overline{S}_{ij}\overline{S}_{ij}]_P$ is the fact that it is based on the discretization adopted in (1) for the viscous and SGS stresses. In particular, the discrete global viscous dissipation resulting from (1) is exactly given by

$$-\sum_P \bar{u}_{i,P}^{n+1/2} \sum_f \nu(\partial_i \bar{u}_j^n + \partial_j \bar{u}_i^{n+1/2})_f \beta_{j,f} A_f, \tag{19}$$

and, in the limit $\Delta t \to 0$, this expression equals $2\nu\sum_P V_P \mathcal{D}[\bar{S}_{ij}\bar{S}_{ij}]_P$ on a discrete basis (see Appendix A). No such property holds if the global dissipation is evaluated through $2\nu\sum_P V_P(\bar{S}_{ij}^n)_P(\bar{S}_{ij}^n)_P$.

Several more sophisticated versions of the Smagorinsky model exist. These include the dynamic Smagorinsky model [21], (variational) multiscale models [9,22], etc. Only the "classical" Smagorinsky model is considered here. Indeed, the aim is to highlight the impact of discretization on the performance of a model and not to compare the quality of several models.

2.3. Simulation parameters

In order to evaluate the performance of the LES discretization and modeling described above, a comparison with pseudo-spectral results from a previous study [23] is performed. The convective term in the pseudo-spectral code is fully de-aliased using the 3/2-truncation rule [24] and the temporal algorithm is based on a 4th-order, low-storage, Runge–Kutta temporal scheme [25]. The subgrid scale term is not de-aliased since it contains the square root of the strain rate and thus cannot be de-aliased. As noted in the introduction, the pseudo-spectral Smagorinsky results have to be considered as the "target" for the finite volume simulations since the pseudo-spectral method offers a very accurate implementation of the LES equations.

In decaying isotropic turbulence, a suitable initial condition can be obtained through the following procedure. First, a high resolution velocity field consisting of 512^3 Fourier modes is built. These modes are initialized so that their amplitudes match the spectra of the Comte–Bellot–Corrsin [26] experiment at stage 1. The phases are initially random and the flow is left to freely decay using direct numerical simulation (i.e. a resolved, non modeled simulation) until the skewness of the velocity derivative reaches a quasi constant value of $S = -0.4$. At this time, the flow is considered "physical". It is then truncated to a resolution of $N = N_x \times N_y \times N_z = 32^3$ modes and the resulting velocity field is used as the LES initial condition. For finite volume simulations, the Fourier field is inverted and evaluated at the control volume centroids (of the dual mesh) to produce the initial condition.

The box size is $L^3 = L_x \times L_y \times L_z = (2\pi)^3$ and the viscosity is set to $\nu = 0.006$ (both L and ν are expressed in SI units). The measured microscale Reynolds number for the initial field is $Re_\lambda = 84.1$ and the Reynolds number based on the integral length-scale is $Re = 380$. In all the figures, time is normalized by the initial eddy-turnover time $\tau_{tu} = 0.238$s.

3. Results – energy decay

3.1. Resolved kinetic energy

The most basic diagnostic for the decay of isotropic turbulence is the resolved global kinetic energy defined by,

$$E_R = \frac{1}{V_{tot}} \int_V \frac{\bar{u}_i \bar{u}_i}{2}\, dV \approx \frac{1}{2V_{tot}} \sum_P \bar{u}_{i,P} \bar{u}_{i,P} V_P, \tag{20}$$

with $V_{tot} = \sum_P V_P$. The simulation results are shown in Fig. 2 while the corresponding symbol legends are defined in Table 1. Aside from the LES runs, filtered DNS (denoted DNS_f in the figure) and unresolved DNS are also presented to emphasize the role of the LES modeling. As is obvious from the figure, unresolved DNS severely underestimate the decay rate of energy.

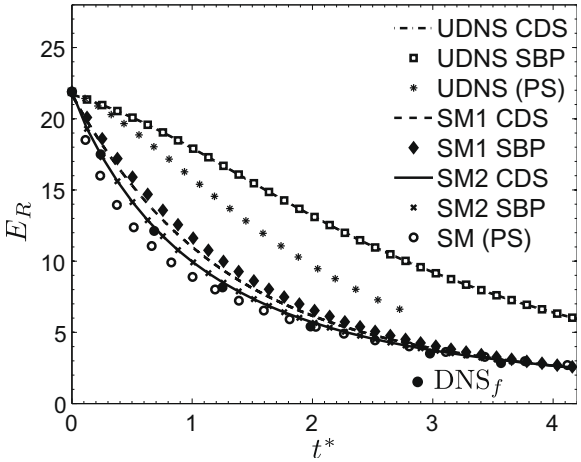

Fig. 2. Time evolution of the resolved kinetic energy. The labels are defined in Table 1.

Table 1
Definition of the symbols used to characterize all the numerical simulation runs.

Label	Numerical scheme	Interpolation method	LES model
SM (PS)	Pseudo-spectral	–	Yes
SM1–CDS	Finite volume	CDS, Eq. (7)	SM1, Eq. (15)
SM1–SBP	Finite volume	SBP, Eq. (8)	SM1, Eq. (15)
SM2–CDS	Finite volume	CDS, Eq. (7)	SM2, Eq. (18)
SM2–SBP	Finite volume	SBP, Eq. (8)	SM2, Eq. (18)
UDNS (PS)	Pseudo-spectral	–	No model
UDNS–CDS	Finite volume	CDS, Eq. (7)	No model
UDNS–SBP	Finite volume	SBP, Eq. (8)	No model

Results obtained with SM2 are significantly better than those obtained using SM1 since they are closer to the spectral predictions (and nearly perfectly match the filtered DNS results). We further note that the interpolation scheme used has very little impact on the results produced using SM2 (the corresponding curves are indistinguishable). On the contrary, the interpolation scheme has a noticeable influence on the predictions made with SM1.

3.2. Viscous and subgrid scale dissipations

The time evolution of the kinetic energy rate is determined by the viscous (ϵ_ν) and subgrid scale (ϵ_{sgs}) dissipation rates. These two quantities have to be computed, respectively, from (19) and the same expression with ν replaced by ν_e in order to get the correct (discrete) balance $dE_R/dt = \epsilon_\nu + \epsilon_{sgs}$. Both dissipation rates are shown in Fig. 3. It is again quite clear that the results obtained with SM2 are more precise than those obtained with SM1, and that the interpolation scheme has almost no influence on the SM2 model predictions. The most important fact is that the subgrid scale dissipation generated by the SM1 model is much too low. Although the SM2 model also underestimates the subgrid scale dissipation at the very beginning of the simulation, its behavior is however significantly closer to spectral results. This of course explains why the SM2 model, compared to the SM1 model, allows a better prediction of the time evolution of the resolved energy (Fig. 2).

3.3. Kinetic energy spectra

The Fourier transform $\bar{u}_i(\mathbf{k})$ of the velocity can be computed from the velocity field known at each grid point in physical space. The energy spectra of the flow is then defined as,

$$E(k) = \frac{1}{2}\int_0^\pi d\theta \int_0^{2\pi} d\varphi k^2 \sin\theta \mid \bar{u}_i(\mathbf{k})\mid^2, \tag{21}$$

where (k, θ, φ) are a spherical coordinate system. Spectra at three different instants during the decay are shown in Fig. 4. Compared to unresolved DNS simulations, all LES runs improve the spectral behavior. Again, the results from the SM2 model are the closest to spectral ones.

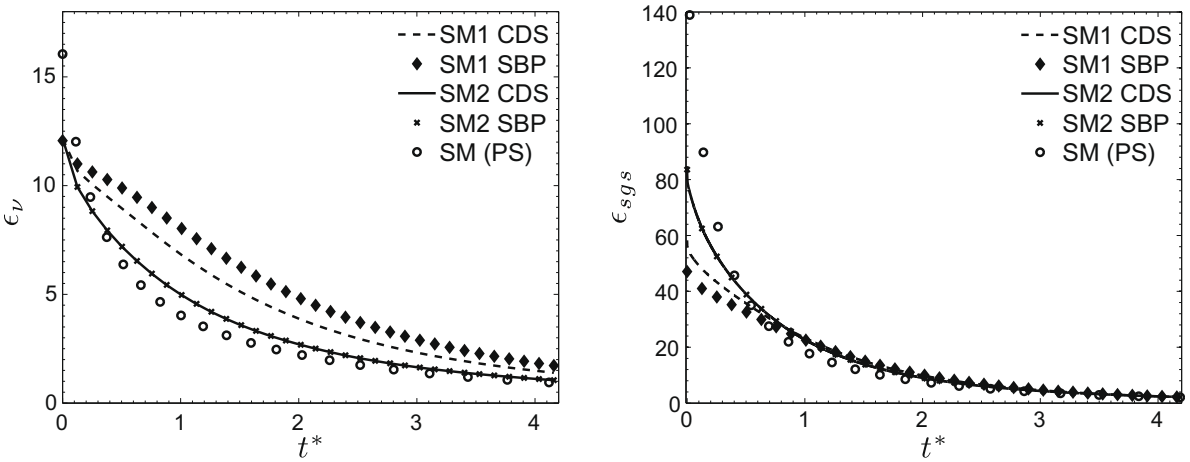

Fig. 3. Time evolution of the viscous (left) and subgrid (right) dissipation rates computed, respectively, from (19) and the same expression with ν replaced by ν_e.

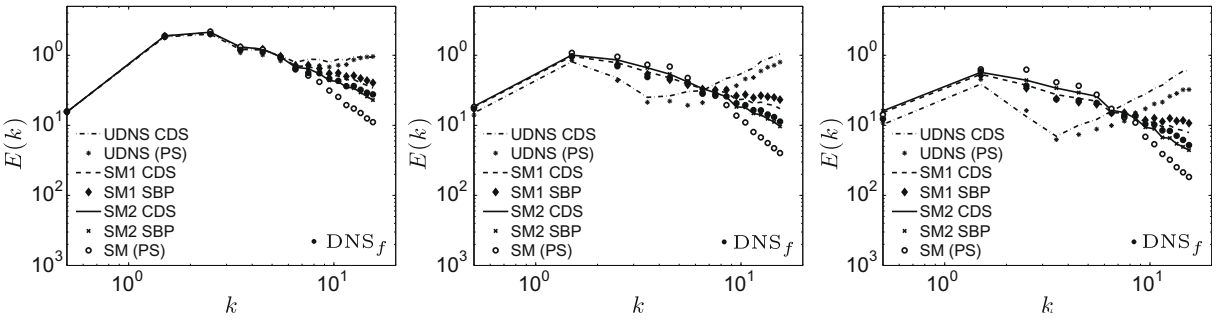

Fig. 4. Kinetic energy spectra measured at three instants during the time evolution. (Left) $t^* = 0.68$; (center) $t^* = 1.98$; and (right) $t^* = 3.56$.

However, even for the SM2 model, the spectra at high wavenumbers do not decay as fast as in the spectral simulation. As stated in the introduction, the emphasis is not put on a comparison with filtered DNS results. We only mention here that the spectra obtained with the SM2 model have the same slope as the filtered DNS spectra at large wavenumbers, as shown by Fig. 4. Therefore, there is no pile-up of energy at high wavenumbers for the run with SM2 model. The results only indicate that the Smagorinsky model, when discretized using the spectral method, is (physically) slightly over-dissipative at scales close to the cut-off.

4. Results – discretization errors

The results of the previous section clearly indicate that compared to the SM1 model, the SM2 model significantly improves finite volume results. At first sight, this statement is quite surprising since they represent discretizations of the same physical model, i.e, the Smagorinsky model. In fact, the only reason why both models differ comes from the presence of large discretization errors. These errors are quantified, a posteriori and a priori, below.

4.1. A posteriori analysis of discretization errors

In Fig. 5 we display the average norm of the strain computed as $\mathcal{S}^{(a)} = \langle (\overline{S}^n_{ij})_P (\overline{S}^n_{ij})_P \rangle$ or $\mathcal{S}^{(b)} = \langle \mathcal{D}[\overline{S}_{ij}\overline{S}_{ij}]_P \rangle$, where the brackets denote spatial averaging. These diagnostics are shown for all the runs, except for the unresolved DNS cases. We observe that $\mathcal{S}^{(a)}$ is systematically much smaller than $\mathcal{S}^{(b)}$ and that it is sensitive to the interpolation scheme adopted (CDS or SBP) even when using the SM2 model.

The difference between $\mathcal{S}^{(a)}$ and $\mathcal{S}^{(b)}$ is not anecdotal. We have seen that taking one discretization or the other greatly influences the efficiency of the subgrid scale model. Equally important is the fact that the interpretation of some physical results might also depend on whether we adopt $\mathcal{S}^{(a)}$ or $\mathcal{S}^{(b)}$ for the discretization of $\langle \overline{S}_{ij}\overline{S}_{ij} \rangle$. For example, the global viscous dissipation rate is usually defined as $\epsilon_v = 2\nu \langle \overline{S}_{ij}\overline{S}_{ij} \rangle$. Depending on whether it is computed as $2\nu \langle (\overline{S}^n_{ij})_P (\overline{S}^n_{ij})_P \rangle$ or $2\nu \langle \mathcal{D}[\overline{S}_{ij}\overline{S}_{ij}]_P \rangle$, the result differs by a factor of 2 or 3 (see Fig. 5).

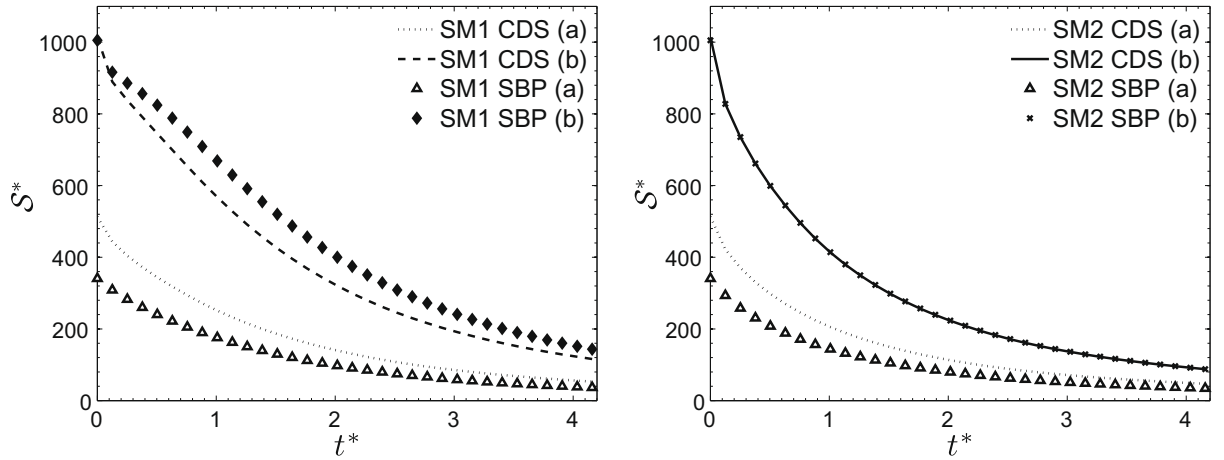

Fig. 5. Time evolution of the average norm of the strain rate computed as $\mathcal{S}^{(a)} = \langle (\overline{S}^n_{ij})_P (\overline{S}^n_{ij})_P \rangle$ (label (a) in the plots) and $\mathcal{S}^{(b)} = \langle \mathcal{D}[\overline{S}_{ij}\overline{S}_{ij}]_P \rangle$ (label (b) in the plots). Results obtained with the SM1 model and the SM2 model are respectively shown in the left and right plots.

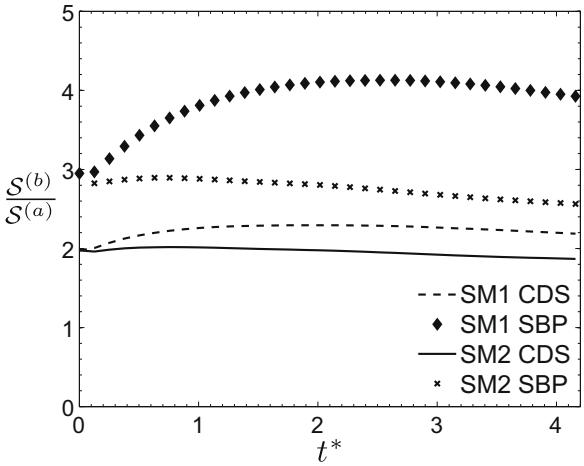

Fig. 6. Time evolution of the ratio $\frac{\mathcal{S}^{(b)}}{\mathcal{S}^{(a)}}$ (used as a measure of discretization errors).

A question that arises is the possibility that the large differences observed in the computation of $\overline{S}_{ij}\overline{S}_{ij}$ through $\mathcal{S}^{(a)}$ or $\mathcal{S}^{(b)}$ are related to our way of initializing the simulations. Indeed, our initial condition is obtained by truncating a 512^3 spectral DNS field to a 32^3 resolution. This produces, on the real space grid, a signal that has sharp gradients and for which it is expected that second-order derivatives cannot be fairly computed. Over time, one could speculate that the numerical solution could evolve towards a state more easily captured by the finite volume discretization and that $\mathcal{S}^{(b)}/\mathcal{S}^{(a)}$ would converge to unity. Fig. 6 shows that this is not the case and we even note an increase of this ratio for the LES runs with the SM1 model. This observation is consistent with earlier results showing that the Smagorinsky model is "under-resolved" with respect to itself [27]. Here we only stress that, as long as the LES cut-off lies in the inertial range (and remains there in the course of time), this is a genuine feature of the LES method.

4.2. A priori analysis of discretization errors

We also use the high resolution DNS database to measure the difference between $\mathcal{S}^{(a)}$ and $\mathcal{S}^{(b)}$. This provides us with an a priori analysis of discretization errors that does not depend on the flow evolution using one model or another.

In Fig. 7 (left), $\mathcal{S}^{(a)}$ and $\mathcal{S}^{(b)}$ are computed on the *same* filtered DNS fields ($512^3 \to 32^3$) at six instants in time ($t^* = 0; 0.24; 0.68; 1.25; 1.98; 3.56$). The norm of the filtered strain computed from the spectral code is also displayed (label DNS_f). As shown, $\mathcal{S}^{(b)}$ systematically provides a better estimation of the average strain rate and it is again almost independent of the interpolation scheme. More quantitatively, we define $\delta_{\mathcal{S}^*} = \mathcal{S}^*/\mathcal{S}^{DNS_f}$ as the fraction of $\mathcal{S}^*$ to the average strain rate computed through the spectral code. As illustrated in Fig. 7(right), $\mathcal{S}^{(b)}$ captures 76% of the average strain rate (for both CDS and

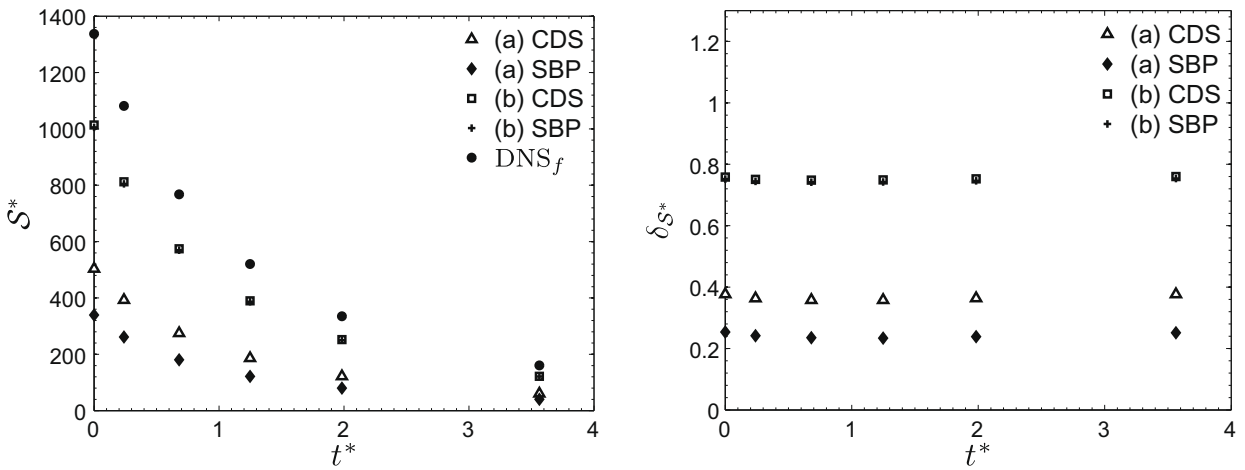

Fig. 7. (Left) Average norm of the strain rate $\mathcal{S}^{(a)}$ and $\mathcal{S}^{(b)}$ computed from the filtered DNS field ($512^3 \to 32^3$) at $t^* = 0; 0.24; 0.68; 1.25; 1.98; 3.56$. (Right) Fraction $\delta_{\mathcal{S}^*}$ of the strain rate captured by the various schemes.

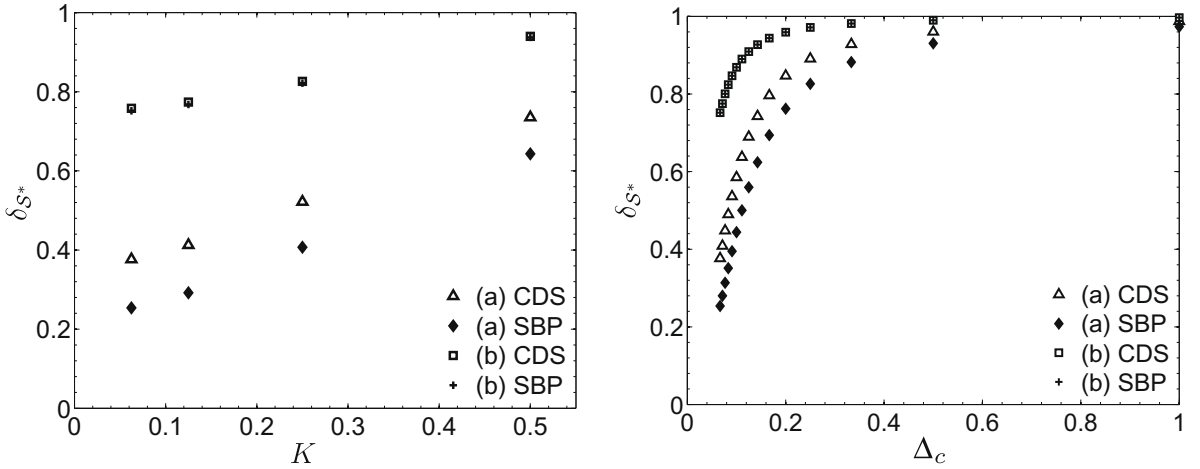

Fig. 8. Fraction δ_{S^*} of the strain rate captured by the various schemes at $t^* = 0$ for different mesh refinements ($N = 32^3, 64^3, 128^3, 256^3$) (left), and different cut-off lengths at $N = 32^3$ (right).

SBP), while $\mathcal{S}^{(a)}$ only captures 38% or 25% of the same quantity depending on whether CDS or SBP interpolations are used. Since $\mathcal{S}^{(a)}$ and $\mathcal{S}^{(b)}$ represent the same physical quantity, we have here an example indicating that on the coarse meshes used in LES, discretization errors can be of the same order of magnitude as the physical quantity measured.

In order to directly link the difference between $(\bar{S}^n_{ij})_P(\bar{S}^n_{ij})_P$ and $\mathcal{D}[\bar{S}_{ij}\bar{S}_{ij}]_P$ to discretization errors, we evaluate $\mathcal{S}^{(a)}$ and $\mathcal{S}^{(b)}$ on the initial DNS field, but filtered down to different resolutions ($32^3, 64^3, 128^3, 256^3$). The corresponding $\delta_{\mathcal{S}^*}$ are plotted in Fig. 8 (left) as a function of the truncation level $K = (N/N_{DNS})^{1/3}$ (defined as the ratio of the filtered resolution to the initial DNS resolution). We observe an increase of δ_{S^*} as K increases for both $\mathcal{S}^{(a)}$ and $\mathcal{S}^{(b)}$. This is of course expected since discretization errors should decrease when the grid is refined. At $N = 256^3$, which is the finer resolution considered here[1], δ_{S^*} reaches 94% for $\mathcal{S}^{(b)}$ (for both interpolation schemes) and 74% (resp. 64%) for $\mathcal{S}^{(a)}$ with CDS (resp. SBP). We also analyze the convergence of $(\bar{S}^n_{ij})_P(\bar{S}^n_{ij})_P$ and $\mathcal{D}[\bar{S}_{ij}\bar{S}_{ij}]_P$ with respect to the resolution by smoothing the velocity field. To that end, we apply a spectral cut-off filter to our initial 32^3 instantaneous velocity field. This spectral cut-off is defined as:

$$\hat{u}_i(\mathbf{k}) = \begin{cases} u_i(\mathbf{k}) & \text{if } |\mathbf{k}| \leqslant k_c \\ 0 & \text{otherwise} \end{cases}, \tag{22}$$

where $k_c = 1/\Delta_c$ is the cut-off wavenumber. This procedure has the advantage of being less demanding in computational resources than the previous mesh refinement. Fig. 8 (right) shows δ_{S^*} as a function of Δ_c (the lowest value of Δ_c corresponds to $k_c = 15$ and the highest value to $k_c = 1$). It is again clear that $\mathcal{S}^{(b)}$ predicts significantly better the average strain rate. As expected, all the methods to measure the strain rate ($\mathcal{S}^{(a)}$, $\mathcal{S}^{(b)}$ and spectral), converge to the same value as the velocity field is filtered and smoothed.

5. Conclusions

In this paper we have discussed two issues related to discretization errors in large eddy simulations. The first one concerns the numerical implementation of Smagorinsky type models. We argue that in order to properly evaluate the norm of the strain and the turbulent viscosity, it is important to consider how the Navier–Stokes equations have been discretized. The implementation we propose is directly derived from the discrete budget of kinetic energy conservation and performs significantly better than the traditional "volume centered" expression. This is clearly due to the fact that the improved formulation (17) is consistent with the discrete strain imposed by the numerical algorithm whereas the "volume centered" expression is not. Although we have focused on homogeneous turbulence, the formulation proposed can be immediately extended to more complex geometries and to other models that use the strain as a scaling. In particular, the dynamic procedure can be used to optimize the Smagorinsky constant C. Extension of our analysis to the case of the channel flow is under preparation.

The second issue we highlighted is the presence of large discretization errors that can be made on diagnostics in LES. For example, we showed that the measurement of viscous dissipation could vary by a factor of 2–3 when using two different discretizations of this diagnostic. Moreover, the quantification of the error with respect to the filtered DNS showed that discretization errors can be of the same order of magnitude as the physical quantity measured. The problem is not related to the

[1] Unfortunately, we could not run the finite volume code at the highest spectral resolution 512^3 because this exceeded our computational capabilities.

absence of subgrid scales in LES simulations (which do not allow a direct comparison with DNS results without filtering or reconstruction). The uncertainty is due to the fact that a LES signal has a significant content at scales close to the grid size and that discrete operators cannot resolve those scales without ambiguity.

As a consequence, it could be concluded that the only way to properly perform an LES is to introduce an explicit filter that strongly damps the signal below the grid size. However, expressions for the subgrid stress tensor related to an explicit filter involve power series in the grid filter size Δ and terms of high-orders in the derivatives of the velocity field [4]. These terms are therefore increasingly difficult to represent on a coarse LES mesh even for filtered signals. In other words, the more a signal is filtered, the more it is difficult to discretize its evolution equations. Furthermore, explicit filtering is difficult to implement for problems involving stretched or skewed meshes. Another option to circumvent the problem of discretization errors, is to use higher-order discretization schemes. These remain accurate for larger grid sizes and are therefore able to better resolve a typical LES signal. Unfortunately, higher-order methods are also difficult to implement and restricted to a limited class of problems. For most practical cases where LES are performed without explicit filtering and with low-order schemes (like 2nd-order), acceptable physics can however be extracted from the simulation as long as the diagnostics considered do not involve scales close to the grid resolution.

Acknowledgments

We are very grateful to the Center For Turbulence Research (Stanford University/ NASA Ames) for allowing us to use their CDP code. We also warmly thank Grégoire Winckelmans and Daniele Carati for fruitful discussions.

A.V. is supported by the Fonds pour la Recherche dans l'Industrie et dans l'Agriculture (F.R.I.A – Belgium). This work, conducted as part of the award (Modeling and simulation of turbulent conductive flows in the limit of low magnetic Reynolds number) made under the European Heads of Research Councils and European Science Foundation EURYI (European Young Investigator) Awards scheme, was supported by funds from the Participating Organisations of EURYI and the EC Sixth Framework Programme. The content of the publication is the sole responsibility of the authors and it does not necessarily represent the views of the Commission or its services. The support of FRS-FNRS Belgium is also gratefully acknowledged.

Appendix A. Relation between $-2\nu\sum_P V_P \mathcal{D}[\bar{S}_{ij}\bar{S}_{ij}]_P$ and the discrete global dissipation

In the limit $\Delta t \to 0$, the discrete global dissipation (19) becomes

$$-\sum_P \bar{u}^n_{i,P} \sum_f \nu(\partial_i \bar{u}^n_j + \partial_j \bar{u}^n_i)_f \beta_{j,f} A_f. \tag{A.1}$$

The superscript n is omitted in the following. Following (17) we also have,

$$2\nu \sum_P V_P \mathcal{D}[\bar{S}_{ij}\bar{S}_{ij}]_P = -\nu \sum_P \bar{u}_{i,P} \sum_f (\partial_i \bar{u}_j + \partial_j \bar{u}_i)_f \beta_{j,f} A_f + \nu \sum_P \sum_f \bar{u}_{i,f} (\partial_i \bar{u}_j + \partial_j \bar{u}_i)_f \beta_{j,f} A_f. \tag{A.2}$$

To show that $2\nu\sum_P V_P \mathcal{D}[\bar{S}_{ij}\bar{S}_{ij}]_P$ is equal to the discrete global dissipation, we thus need to prove that $\sum_P \sum_f \bar{u}_{i,f}(\partial_i \bar{u}_j + \partial_j \bar{u}_i)_f \beta_{j,f} A_f = 0$ (up to a boundary contribution which vanishes in the periodic case).

Using the definition of the face variables and the velocity derivatives, we have,

$$\sum_P \sum_f \bar{u}_{i,f}(\partial_i \bar{u}_j + \partial_j \bar{u}_i)_f \beta_{j,f} A_f = \sum_P \sum_f \frac{(\bar{u}_{i,P} + \bar{u}_{i,nbr})}{2} \frac{(\bar{u}_{i,nbr} - \bar{u}_{i,P})}{\|x_{j,nbr} - x_{j,P}\|} A_f + \sum_P \sum_f \frac{(\bar{u}_{i,P} + \bar{u}_{i,nbr})[(\partial_i \bar{u}_j)_P + (\partial_i \bar{u}_j)_{nbr}]}{4} \beta_{j,f} A_f$$

In both sums, all internal boundaries contribute twice with an opposite contribution for the two control volumes they delimit. Indeed, in the first (resp. second) sum, $\bar{u}_{i,nbr} - \bar{u}_{i,P}$ (resp. $\beta_{j,f}$) changes sign for two neighboring volumes while the other terms remain identical. The second term on the rhs of (A.2) is thus a boundary term as required.

References

[1] B. Vreman, B. Geurts, J. Kuerten, Discretization error dominance over subgrid terms in large eddy simulation of compressible shear layers in 2D, Commun. Numer. Methods Eng. 10 (1995) 785–790.
[2] S. Ghosal, An analysis of numerical errors in large-eddy simulations of turbulence, J. Comput. Phys. 125 (1996) 187–206.
[3] F. Chow, P. Moin, A further study of numerical errors in large-eddy simulations, J. Comput. Phys. 184 (2003) 366–380.
[4] D. Carati, G. Winckelmans, H. Jeanmart, On the modelling of the subgrid-scale and filtered-scale stress tensors in large-eddy simulation, J. Fluid Mech. 441 (2001) 119–138.
[5] R. Rogallo, P. Moin, Numerical simulation of turbulent flows, Annu. Rev. Fluid Mech. 16 (1984) 99–137.
[6] G. Winckelmans, A. Wray, O. Vasilyev, H. Jeanmart, Explicit-filtering large-eddy simulation using the tensor-diffusivity model supplemented by a dynamic Smagorinsky term, Phys. Fluids 13 (5) (2001) 1385–1403.
[7] T. Lund, The use of explicit filters in large eddy simulation, Comput. Math. Appl. 46 (2003) 603–616.
[8] O. Vasilyev, T. Lund, P. Moin, A general class of commutative filters for LES in complex geometries, J. Comput. Phys. 146 (1998) 82–104.
[9] T. Hughes, A. Oberai, L. Mazzei, Large eddy simulation of turbulent channel flows by the variational multiscale method, Phys. Fluids 13 (6) (2001) 1784–1799.
[10] H. Jeanmart, G. Winckelmans, Investigation of eddy-viscosity models modified using discrete filters: a simplified "regularized variational multiscale model" and an "enhanced field model", Phys. Fluids 19 (2007) 055110.
[11] B. Geurts, J. Fröhlich, A framework for predicting accuracy limitations in large-eddy simulation, Phys. Fluids 14 (6) (2002) L41–L44.

[12] J. Meyers, B. Geurts, M. Baelmans, Database analysis of errors in large-eddy simulation, Phys. Fluids 15 (9) (2003) 2740–2755.
[13] J. Meyers, B. Geurts, M. Baelmans, Optimality of the dynamic procedure for large-eddy simulations, Phys. Fluids 17 (2005) 045108.
[14] J. Meyers, B. Geurts, P. Sagaut, A computational error-assessment of central finite-volume discretizations in large-eddy simulation using a Smagorinsky model, J. Comput. Phys. 227 (2007) 156–173.
[15] B. Vreman, B. Geurts, H. Kuerten, Comparison of numerical schemes in large-eddy simulation of the temporal mixing layer, Int. J. Numer. Methods Fluids 22 (1996) 297–311.
[16] K. Mahesh, G. Constantinescu, S. Apte, G. Iaccarino, F. Ham, P. Moin, Progress toward large-eddy simulation of turbulent reacting and non-reacting flows in complex geometries, in: Annual Research Briefs, Center for Turbulence Research, NASA Ames/Stanford University, 2002, pp. 115–142.
[17] F. Ham, G. Iaccarino, Energy conservation in collocated discretization schemes on unstructured meshes, in: Annual Research Briefs, Center for Turbulence Research, NASA Ames/Stanford University, 2004, pp. 3–14.
[18] F. Ham, K. Mattsson, G. Iaccarino, Accurate and stable finite volume operators for unstructured flow solvers, in: Annual Research Briefs, Center for Turbulence Research, NASA Ames/Stanford University, 2006, pp. 243–261.
[19] J. Smagorinsky, General circulation experiments with the primitive equations: 1. The basic experiment, Mon. Weather Rev. 91 (1963) 99–164.
[20] S. Pope, Turbulent Flows, Cambridge University Press, 2000.
[21] M. Germano, U. Piomelli, P. Moin, W. Cabot, A dynamic subgrid-scale eddy viscosity model, Phys. Fluids A 3 (7) (1991) 1760–1765.
[22] R. Cocle, Combining the Vortex-in-cell and Parallel Fast Multipole Methods for Efficient Domain Decomposition Simulations: DNS and LES Approaches, Ph.D. Thesis, Université Catholique de Louvain, August 2007.
[23] B. Knaepen, P. Moin, Large-eddy simulation of conductive flows at low magnetic Reynolds number, Phys. Fluids 16 (2004) 1255–1261.
[24] S.A. Orszag, On the elimination of aliasing in finite-difference schemes by filtering high-wavenumber components, J. Atmos. Sci. 28 (1971) 1074.
[25] J. Williamson, Low-storage Runge–Kutta schemes, J. Comput. Phys. 35 (1980) 48–56.
[26] G. Comte-Bellot, S. Corrsin, Simple eulerian time correlations of full- and narrow-band velocity signals in grid generated 'isotropic' turbulence, J. Fluid Mech. 48 (1971) 273–337.
[27] G. Daeninck, Developments in Hybrid Approaches, Ph.D. Thesis, Université Catholique de Louvain, December 2006.